Heinonen, J.S., Fusswinkel, T. 2017. High Ni and low Mn/Fe in olivine phenocrysts of the Karoo meimechites do not reflect pyroxenitic mantle sources. Chemical Geology 467, 134–142. https://doi.org/10.1016/j.chemgeo.2017.08.002 (Author's postprint)

High Ni and low Mn/Fe in olivine phenocrysts of the Karoo meimechites do not reflect pyroxenitic mantle sources

Jussi S. Heinonen (PhD, corresponding author, jussi.s.heinonen@helsinki.fi, +358-50-3185304)
Tobias Fusswinkel (PhD, tobias.fusswinkel@helsinki.fi, +358-50-4160671)

Department of Geosciences and Geography, P.O. Box 64, University of Helsinki, 00014, Helsinki, Finland

Abstract
Nickel contents and Mn/Fe in olivine phenocrysts have been suggested to reflect the mineral composition of the mantle source of the host magma. This hypothesis is tested here against a well-characterized suite of meimechitic (or Ti-rich komatiitic) dikes from the Antarctic extension of the Jurassic ~180 Ma Karoo large igneous province. The presented trace element data on $Fo_{82–92}$ olivines show relatively high Ni (2430–3570 ppm) and low 100*Mn/Fe (1.32–1.5; Mn = 890–1570 ppm), compatible with pyroxenite-rich sources (X_{px} = 37–75%). Many other mantle source indicators (parental melt MgO and whole-rock Zn/Fe, MgO/CaO, FC3MS, Zr/Y vs. Nb/Y, and radiogenic isotope compositions) suggest dominantly or solely peridotitic mantle sources, however. Therefore, the measured high Ni and low Mn/Fe are likely to reflect high temperatures and pressures of melting and possibly high water contents in such peridotite sources. We recommend considerable caution when using Ni and Mn contents of olivine as source indicators, as they may only serve for qualitative comparison of primitive volcanic rocks that originated under fairly similar mantle conditions.

Keywords: olivine; LA-ICP-MS; trace elements; nickel; manganese; mantle sources; pyroxenite; peridotite; recycled crust; large igneous provinces; Karoo

1. Introduction

Mantle pyroxenite may form by reactions between recycled crust (subducted eclogite) and mantle peridotite. Whether Mg-rich volcanic rocks, especially in various intraplate settings, originate dominantly from pyroxenitic or peridotitic mantle sources has been debated (e.g., Putirka, 1999; Sobolev et al., 2005, 2007; Niu et al., 2011; Putirka et al., 2011, Yang and Zhou, 2013).

In a study concerning Hawaiian shield basalts, Sobolev et al. (2005) first suggested the suitability of Ni contents of olivine phenocrysts as an indicator of mineral composition of the mantle source of their host magma. Later, based on considerations of partition coefficients and vast amounts of olivine analyses from various tectonic settings, Sobolev et al. (2007) suggested that the amount of pyroxenite in the mantle source could be quantified on the basis of Mn/Fe of olivine phenocrysts. The underlying hypotheses suggest that, in an olivine-poor mantle source, Ni behaves as an incompatible element and Mn as a compatible element (relative to Fe). Magmas derived from pyroxenite would thus exhibit higher Ni contents and lower Mn/Fe relative to those derived from peridotite, and these features would then be recorded by olivine phenocrysts crystallizing from the magma at lower pressures. Following this logic and utilizing the extensive olivine dataset, Sobolev et al. (2007) suggested that some large igneous provinces (LIPs) could have originated dominantly from pyroxenitic sources whereas mid-ocean ridge basalts (MORBs) derive from sources consisting of about 10–15 % of pyroxenite.

Because of the relative ease of analyzing trace elements in olivine, the aforementioned approaches have been widely used in identification of the mantle sources of various volcanic successions (e.g., Kamenetsky et al., 2012; Garcia et al., 2015; Søager et al., 2015). In some cases, these indicators have shown correlations with other chemical parameters that potentially indicate recycled sources, e.g., Os isotopes (Sobolev et al., 2008).

Subsequent experimental and theoretical studies on element partitioning during peridotite melting, however, have suggested that temperature (and, indirectly, pressure) as well as water contents of the mantle source have a strong effect on partitioning of Ni and Mn (Li and Ripley, 2010; Balta et al., 2011; Niu et al., 2011; Matzen et al., 2013, 2017). For example, higher melting temperatures and pressures decrease the partition coefficient of Ni between olivine and liquid ($K_D(Ni)^{ol\text{-}liq}$) and increase $K_D(Mn)^{ol\text{-}liq}$ (Li and Ripley, 2010; Matzen et al., 2013, 2017) whereas higher water content of the source increases $K_D(Mn)^{garnet\text{-}liq}$ (Balta et al., 2011). The effects of these parameters on the magma Ni and Mn contents could exceed the effects caused by variations in source mineralogy and also explain the apparent differences in olivine chemistry between MOR and LIP basalts (Balta et al., 2011; Matzen et al., 2017).

In this study, major and trace element data on olivine phenocrysts from a suite of subalkaline Mg-rich dikes that belong to the Antarctic portion of the Jurassic (~180 Ma; Jourdan et al., 2005) Karoo LIP are presented (Fig. 1). These rocks have been extensively studied using major element, trace element, isotopic (Sr, Nd, Pb, Os, He), and mineral major element chemistry (Heinonen and Luttinen, 2008, 2010; Heinonen et al., 2010; Heinonen and Kurz, 2015). They do not exhibit geochemical evidence of highly metasomatized sources, magma mixing, or significant lithospheric interaction, and were derived at high pressures from depleted mantle sources beneath the Gondwanan lithosphere. As such, they provide an excellent natural testing laboratory for behavior of Mn and Ni in mantle melting. On the basis of the new and previously published data, the plausibility of olivine Ni and Mn contents as tracers of mantle source mineral composition is discussed.

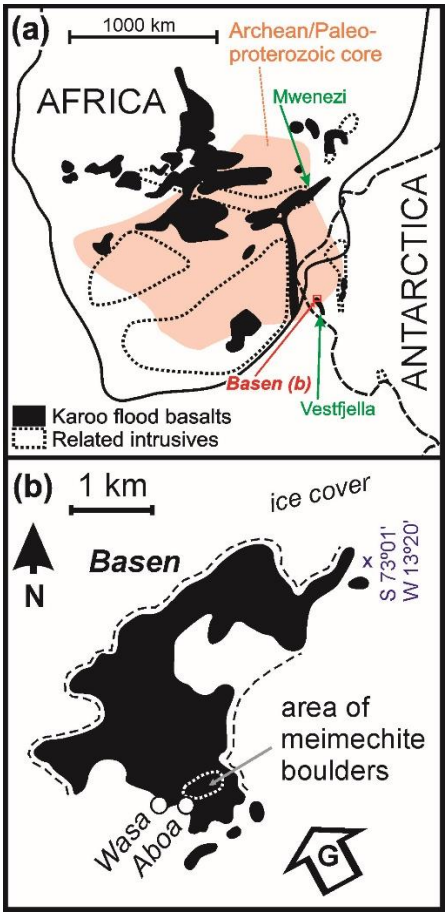

Figure 1. (a) Reconstruction of Africa and Antarctica at ~180 Ma showing the present-day distribution of Karoo CFBs and related intrusive rocks (Luttinen and Siivola 1997; Jourdan et al. 2007) and the Archean/Paleoproterozoic core complex of Kalahari (Jacobs et al. 2008). (b) Detailed map of Basen nunatak, Vestfjella. Arrow marked with "G" indicates the approximate primary ice flow direction and stippled lines indicate steep cliffs. The locations of Aboa (Finnish) and Wasa (Swedish) research stations are also indicated.

2. Geological background and sample selection

The Karoo LIP is one of the largest flood basalt provinces, and is related to the breakup of Pangaea and Gondwana supercontinents. Most of its remains are found in southern Africa, but parts of it have also been preserved in Antarctica (Fig. 1). The most MgO-rich (> 20 wt. %) magmas known from the Karoo LIP have left their geochemical fingerprints in glacial boulders that are found scattered on top of Basen nunatak in the Vestfjella mountain range, western Dronning Maud Land, Antarctica (Fig. 1; Heinonen and Luttinen, 2010). The Basen nunatak itself consists of Karoo continental flood basalts (CFBs), but the boulders contain chilled-margin contacts with Permian sedimentary rocks that underlie the CFBs at places in Vestfjella – therefore the boulders have likely been transported from the surrounding valleys on top of the nunatak by glaciers. Because of glacial erosion in sub-zero conditions, many of these boulders are free of notable chemical weathering and the primary mineral and geochemical compositions have been preserved exceptionally well. For example, olivine phenocrysts are often pristine.

The boulders are classified as picrites and meimechites according to the revised classification of high-Mg rocks by Le Bas (2000), although it is important to note that the rocks are subalkaline and distinct from the alkaline and considerably incompatible trace element-enriched meimechites from the type locality in Siberia (see, e.g., Arndt et al., 1995). A more petrogenetically appropriate term would probably be "Ti-rich komatiite" as the TiO_2 contents (1.3–1.7 wt. %) of the samples are very close to the TiO_2 concentration boundary of 1 wt. % between a komatiite and a meimechite (see Le Bas, 2000). For comparison, Siberian meimechites have TiO_2 contents of more than 3 wt. % at similar MgO contents (Arndt et al., 1995). We follow the nomenclature that is recommended by IUGS (Le Bas, 2000) and used in previous publications about these rocks (e.g., Heinonen and Luttinen, 2010), however.

Although a few of the Karoo meimechite samples from Vestfjella are obvious cumulates, some of them are characterized by considerably magnesian olivine phenocrysts (up to Fo_{92}) that indicate crystallization from parental magmas having MgO in excess of 20 wt. %, possibly up to 25 wt. % (Heinonen and Luttinen, 2010). These meimechites are geochemically closely associated with ferropicritic dikes, which are also found at Vestfjella, share the same mantle source, and may have differentiated from meimechitic parental magmas similar to those represented by the boulders (Heinonen and Luttinen, 2010: Heinonen et al., 2010). In contrast to Mwenezi picrites found in southern Africa (Fig. 1a) that show evidence of significant mixing with or derivation from geochemically enriched lithospheric materials (e.g., Ellam, 2006), the meimechites and related ferropicrites of Vestfjella have been shown to derive from depleted sublithospheric sources beneath the Gondwanan supercontinent (Heinonen et al., 2010; Heinonen and Kurz, 2015). Two of the meimechite samples that contain the most pristine olivine, AL/B7-03 (MgO = 19 wt. %) and AL/B9-03 (MgO = 24 wt. %), were selected for this study (see Heinonen and Luttinen, 2008, 2010).

3. Analytical methods

The whole-rock samples were crushed and the least altered olivine grains were hand-picked from sieved (Ø = 0.25–1 mm) and magnetically separated fractions. The grains were mounted, polished, and gold-coated for oxygen isotopic analysis, and these mounts were also used in this study.

3.1 Electron probe microanalysis

Major element compositions of olivine used for calibration of the laser ablation-inductively coupled plasma-mass spectrometry (LA-ICP-MS; see next section) data were determined at the Department of Geosciences and Geography, University of Helsinki, with a JEOL JXA-8600 electron probe micro-analyzer (EPMA) equipped with four wavelength-dispersive spectrometers. Matrix corrections were performed with the XMAS analysis software using the PAP correction (Pouchou

and Pichoir, 1985). The microprobe was calibrated with an olivine standard. The analyses were performed with a focused beam, and the acceleration voltage and sample current for the analyses were 15 kV and 15 nA, respectively. The precision and limit of detection for the method is reported in Electronic Supplementary Materials.

3.2 LA-ICP-MS analysis

LA-ICP-MS analyses were carried out at the University of Helsinki using an Agilent 7900s quadrupole ICP-MS system equipped with high-sensitivity (s-lens) ion lens configuration and Pt interface cones. The instrument is coupled to a Coherent GeoLas Pro MV 193 nm laser ablation system. The system was tuned daily to ensure highest possible signal-to-background ratios while maintaining low oxide interference production ratios (ThO/Th < 0.3 %), low doubly charged formation ($^{43}Ca^{2+}/^{43}Ca$ < 0.5 %) and stable ablation, transport and ionization conditions (U/Th = 100±2 %). The accuracy of the system was monitored daily by replicate analyses of 39 elements in NISTSRM 612 synthetic glass standards quantified against NISTSRM 610 as external standard. Accuracies for major and trace elements were within or very close (< 5 % relative deviation) to the propagated uncertainty ranges associated with the reference standard compositions (Spandler et al., 2011). Other instrument parameters and gas flow rates are summarized in Table 1.

Table 1. Summary of instrumental parameters used for olivine LA-ICP-MS analysis

Laser system	Coherent GeoLas Pro MV
Wavelength	193 nm
Laser fluence	7 J/cm²
Repetition rate	10 Hz
Crater size	44 µm circular spots
ICP-MS	Agilent 7900s
He Carrier gas flow	1.0 l/min
He Auxiliary gas flow	0.85 l/min
Ar Plasma gas flow	15 l/min
RF power	1500 W
ThO/Th	Tuned to < 0.3 %
U/Th	Tuned to ~ 100 %
$^{43}Ca^{2+}/^{43}Ca$	Tuned to < 0.5 %
Isotopes measured	^{24}Mg, ^{27}Al, ^{29}Si, ^{43}Ca, ^{44}Ca, ^{49}Ti, ^{51}V, ^{52}Cr, ^{55}Mn, ^{56}Fe, ^{57}Fe, ^{59}Co, ^{60}Ni, ^{62}Ni, ^{63}Cu, ^{66}Zn
Dwell time per mass	10 ms

The olivine samples were ablated at the location of the EPMA analysis spots using spot sizes of 44 µm and laser energy densities of 7 J/cm^2. The olivine analyses were bracketed by replicate measurements of reference materials NISTSRM 610 (Spandler et al., 2011) and GSE 1G (GeoREM preferred values, Jochum et al., 2005) at laser energies of 10 J/cm². The following isotopes were included in the measurement program: ^{24}Mg, ^{27}Al, ^{29}Si, ^{43}Ca, ^{44}Ca, ^{49}Ti, ^{51}V, ^{52}Cr, ^{55}Mn, ^{56}Fe, ^{57}Fe, ^{59}Co, ^{60}Ni, ^{62}Ni, ^{63}Cu, ^{66}Zn. Data reduction was carried out using the SILLS software package (Guillong et al., 2008), following procedures outlined in Heinrich et al. (2003) and Pettke et al. (2012). Based on careful evaluation of data quality and accuracy (see Electronic Supplementary Material), Mg concentration values as determined with EPMA were used for internal standardization of the data against GSE 1G synthetic basalt glass as external standard.

4. Results

The results of our major and trace element analyses on olivine phenocrysts ($Fo_{82–92}$) of the Karoo meimechites are given in Table 2 (LA-ICP-MS) and Electronic Supplementary Material (LA-

Heinonen, J.S., Fusswinkel, T. 2017. High Ni and low Mn/Fe in olivine phenocrysts of the Karoo meimechites do not reflect pyroxenitic mantle sources. Chemical Geology 467, 134–142. https://doi.org/10.1016/j.chemgeo.2017.08.002 (Author's postprint)

Table 2. Weighted means of LA-ICP-MS compositional data of Karoo olivine grains, using the 1σ errors of the LA-ICP-MS analyses as weighting factors (see Electronic Supplementary Materials). Uncertainties of means are given in italics. Weighted means and uncertainties were rounded to appropriate numbers of significant digits. All concentrations in µg/g (ppm).

Sample	Fo (%)	Mg*	Fe	Si	Al	Ca	Ti	V	Cr	Mn	Co	Ni	Cu	Zn	100*Mn/Fe	X_{px} (%)	X_{crc} (%)
B7-13	91.4	297220	59900	179000	468	2029	71	5.3	1166	887	154	2947	5.1	64	1.48	41	12
$\sigma_{\bar{x}}$		*3900*	*730*	*2300*	*6*	*35*	*1*	*0.1*	*15*	*11*	*2*	*26*	*0.1*	*1*			
B7-11	91.9	298640	59900	181000	419	1880	72	4.9	860	900	143	3570	4.7	65	1.5	37	10
$\sigma_{\bar{x}}$		*4600*	*870*	*2400*	*6*	*35*	*1*	*0.1*	*14*	*14*	*2*	*44*	*0.1*	*1*			
B7-10	90.3	292650	67200	179800	438	1970	69	5.1	1090	990	150	3150	4.9	69	1.47	44	13
$\sigma_{\bar{x}}$		*3800*	*860*	*2200*	*5*	*31*	*1*	*0.1*	*13*	*12*	*2*	*34*	*0.1*	*1*			
B7-9	89.9	290590	72000	178400	392	1890	78	6.3	940	1040	160	3180	5.7	73	1.44	50	15
$\sigma_{\bar{x}}$		*4400*	*1120*	*2500*	*5*	*35*	*1*	*0.1*	*16*	*18*	*2*	*40*	*0.1*	*1*			
B7-5	90.5	290660	67800	177000	393	1930	58	5.2	1010	990	154	3300	5.2	71	1.46	46	14
$\sigma_{\bar{x}}$		*3900*	*840*	*2100*	*4*	*32*	*1*	*0.1*	*13*	*13*	*2*	*36*	*0.1*	*1*			
B7-1	91.3	294810	63400	180600	467	1870	86	5.7	930	920	143	3520	4.9	69	1.44	50	15
$\sigma_{\bar{x}}$		*3700*	*690*	*2100*	*6*	*28*	*1*	*0.1*	*11*	*10*	*2*	*35*	*0.1*	*1*			
B9-11	90.2	293130	70500	180200	436	1900	79	5.8	890	1000	152	3430	5.1	76	1.42	54	17
$\sigma_{\bar{x}}$		*3800*	*850*	*2100*	*6*	*31*	*1*	*0.1*	*12*	*12*	*2*	*34*	*0.1*	*1*			
B9-10	90.4	291700	67900	178900	497	1920	85	6.7	950	980	148	3320	4.7	73	1.44	50	16
$\sigma_{\bar{x}}$		*3600*	*810*	*2200*	*6*	*31*	*1*	*0.1*	*12*	*13*	*2*	*32*	*0.1*	*1*			
B9-7	90.2	289640	69800	177400	396	1870	76	6.1	810	970	150	3510	4.8	76	1.39	59	20
$\sigma_{\bar{x}}$		*3700*	*840*	*2100*	*5*	*31*	*1*	*0.1*	*11*	*12*	*2*	*37*	*0.1*	*1*			
B9-6	84.7	268460	108700	175400	338	2510	86	8.6	410	1530	180	2430	6.4	100	1.41	56	19
$\sigma_{\bar{x}}$		*3400*	*1240*	*2100*	*4*	*39*	*1*	*0.1*	*5*	*17*	*2*	*25*	*0.1*	*1*			
B9-5	90.4	291840	69300	181200	476	1940	84	6.6	950	980	152	3390	4.9	74	1.42	54	18
$\sigma_{\bar{x}}$		*4100*	*940*	*2400*	*7*	*31*	*1*	*0.1*	*12*	*13*	*2*	*37*	*0.1*	*1*			
B9-4	83.6	263800	111800	172300	372	2370	86	11	650	1570	177	2550	4.7	113	1.4	58	20
$\sigma_{\bar{x}}$		*3400*	*1390*	*2200*	*5*	*35*	*1*	*0.2*	*10*	*20*	*2.*	*28*	*0.1*	*2*			
B9-2	88.6	285690	82300	180300	465	1920	88	7.6	840	1170	169	3120	5.5	79	1.42	55	18
$\sigma_{\bar{x}}$		*3600*	*930*	*2300*	*6*	*31*	*1*	*0.1*	*11*	*14*	*2*	*32*	*0.1*	*1*			
B9-1	85.9	273240	98800	177000	415	2250	70	9.4	640	1300	167	2840	7.7	115	1.32	75	31
$\sigma_{\bar{x}}$		*3800*	*1200*	*2500*	*5*	*41*	*1*	*0.1*	*10*	*17*	*2*	*32*	*0.1*	*1*			

* Determined by EPMA, used for internal standardization of LA-ICP-MS analyses

ICP-MS and EPMA), and illustrated in Fig. 2. The data shows similarity to olivines from oceanic island basalts (OIBs) and LIPs erupted on thick lithosphere by having relatively high Ni (2430–3570 ppm) and low 100*Mn/Fe (1.32–1.5; Mn = 890–1570 ppm) at a given Fo content (Fig. 2). Calcium (1870–2030 ppm) and Co (143–169 ppm) contents of the most primitive Karoo meimechite olivines (>Fo_{86}) are also similar to values measured from olivines of volcanic rocks erupted on thick lithosphere at similar Fo contents (1000–2500 ppm and 130–170 ppm, respectively; Sobolev et al., 2007).

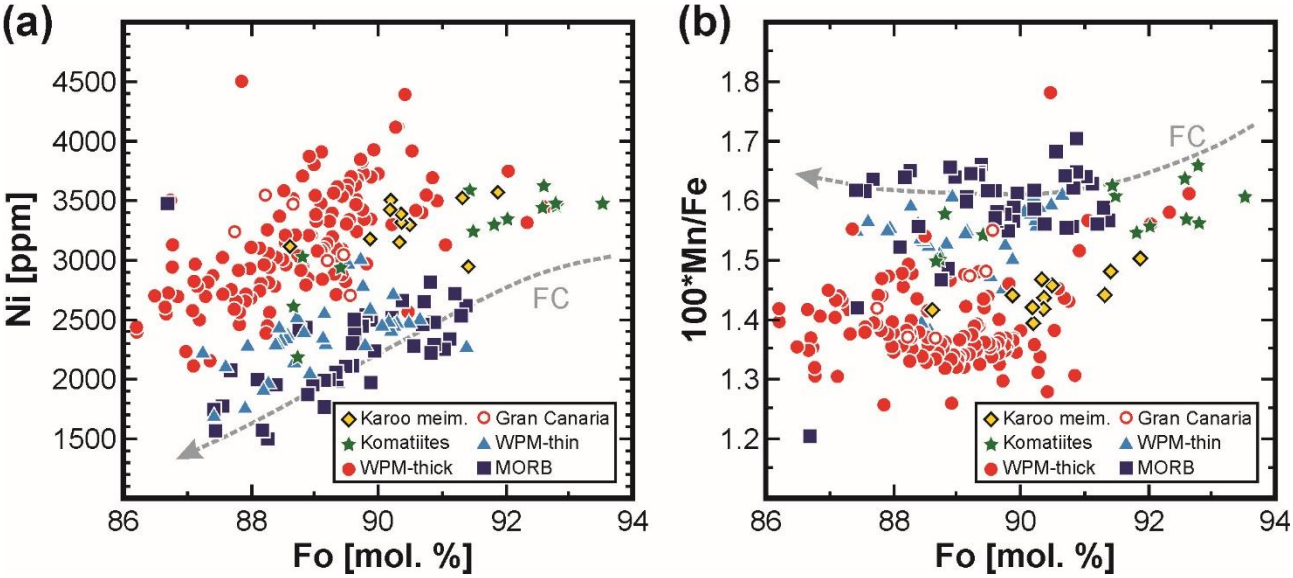

Figure 2. Olivine compositions of Karoo meimechites shown in (a) Fo [mol. %] vs. Ni [ppm] and (b) Fo [mol. %] vs. 100*Mn/Fe diagrams. Data for Archean komatiites, within-plate magmas emplaced over thick lithosphere (> 70 km; WPM-thick), Gran Canaria picrites (highlighted subclass of WPM-thick), within-plate magmas emplaced over thin lithosphere (< 70 km; WPM-thin), and MORBs shown for comparison (Sobolev et al., 2007). Fractional crystallization model (FC) of a melt derived from fertile peridotite is after Frac-2 model of Sobolev et al. (2007). Note that a couple of the analyses presented in Table 2 have Fo contents so low that they plot outside the diagrams – we focus on the most Mg-rich compositions here as they are most relevant to the discussion.

Sobolev et al. (2007) provided equations to calculate the amount of pyroxenite (X_{px}) and recycled oceanic crust (X_{crc}) in the mantle source using Fe, Mn, and standardized information on the behavior of different mantle rock types under melting conditions relevant to different tectonic environments:

$$X_{px} = 3.48 - 2.071 * (100 * \frac{\mathrm{Mn}}{\mathrm{Fe}}) \quad (1)$$

and

$$X_{crc} = \frac{X_e}{F_e\left(\frac{1-X_{px}}{X_{px}} * \frac{F_{px}}{F_{pe}} + \frac{1-F_e}{F_e} * X_e + 1\right)} \quad (2)$$

In (2), F_e is the degree of melting of recycled eclogite, X_e is the amount of eclogite-derived melt needed to produce hybrid pyroxenite from peridotite, and F_{pe} and F_{px} are degrees of melting of peridotite and pyroxenite, respectively. Following Sobolev et al. (2007), we adopt the following standard values that are relevant to a LIP setting: F_e = 50 %, X_e = 50 %, F_{px} = 50 %, and F_{pe} = 10 %. Combining equations (1) and (2) with the LA-ICP-MS data we get X_{px} of 37–75 % with an average of 52% (1σ = 9 %) and X_{crc} of 10–31 % with an average of 17 % (1σ = 5 %) (Fig. 3) for all olivines. Sample-specific average X_{px} and X_{crc} values are 45 % and 13 % for AL/B7-03 and 58 % and 20 % for

AL/B9-03, respectively. Very similar X_{px} values (52 % on average) were reported for the basalts of Gran Canaria (OIBs erupted on thick lithosphere) by Sobolev et al. (2007) (Fig. 3).

The picrite samples reported from the African Karoo (Mwenezi) by Sobolev et al. (2007) also exhibit rather similar X_{px} values (62 % on average) with Karoo meimechites (Fig. 3). We emphasize, that direct comparison in this case is not justified, however, as trace element and isotopic (Sr, Nd, Pb, and Os) evidence indicates derivation of these Karoo magma types dominantly from distinct magma sources in the enriched continental lithospheric mantle and depleted asthenosphere, respectively (see, e.g., Heinonen et al., 2010). The relationships of these magma types to each other and Karoo magmatism in general have been discussed elsewhere (e.g., Ellam, 2006; Heinonen et al., 2010, 2016; Heinonen and Kurz, 2015; Luttinen et al., 2015) and will not be considered further in this study.

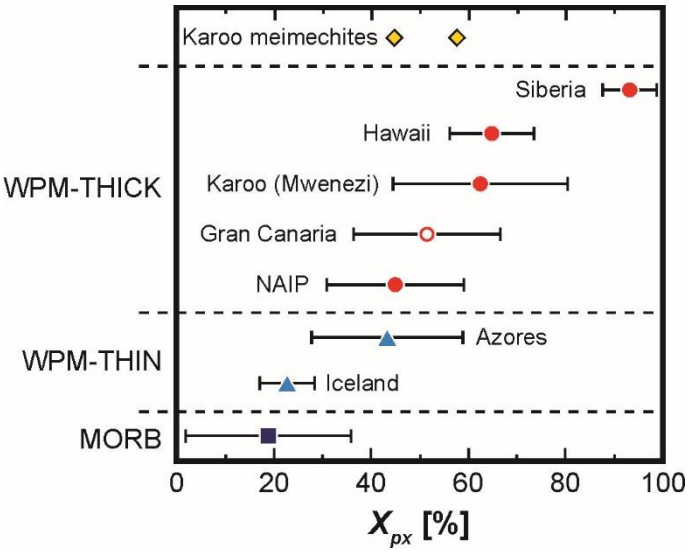

Figure 3. The amount of pyroxenite in the mantle source (X_{px}) calculated on the basis of Mn/Fe of olivine phenocrysts for Karoo meimechites (this study) and picrites and basalts from Siberian Traps LIP, Hawaii, African Karoo LIP (Mwenezi), Gran Canaria, NAIP (Northern Atlantic Igneous Province), Azores, Iceland, and MORBs (Sobolev et al., 2007). Symbols for the Karoo meimechites represent X_{px} values calculated on the basis of average olivines of the two whole-rock samples analyzed here (AL/B7-03 and AL/B9-03) and the symbols for the other locations represent the average X_{px} values of all of the whole-rock samples with the error bars illustrating the standard deviation. WPM-thick and WPM-thin classification as in Fig. 2.

5. Discussion

5.1. Evidence from other pyroxenite and recycled source indicators

The olivine Ni and Mn/Fe data of the Karoo meimechites suggest dominantly pyroxenitic sources for these primitive rocks (Figs. 2 and 3). Geoscientists are not solely dependent on these pyroxenite tracers, however. Although lithological and geochemical heterogeneity do not necessarily go hand in hand (e.g., Yang and Zhou, 2013; Matzen et al., 2017), several potential indicators of pyroxenite or recycled sources have been introduced. These include Zn/Fe (Le Roux et al., 2010), MgO/CaO (Herzberg, 2006; Herzberg and Asimow, 2008), FC3MS (Yang and Zhou, 2013), Zr/Y vs. Nb/Y (Fitton et al., 1997), and radiogenic isotope compositions (e.g., Hofmann and White, 1982). In addition, several other major element characteristics of magmas can be associated with pyroxenite sources: for thorough reviews of the different tracers and potential pitfalls in using them, the reader is referred to Yang et al. (2016). Importantly, Karoo meimechites are subalkaline and do not show significant evidence of magma mixing, highly metasomatized sources, or interaction with lithospheric materials (Heinonen and Luttinen, 2010; Heinonen et al., 2010), which means that many of the problems related to the geochemical outcomes of such processes (Yang et al., 2016) are not relevant to this study.

Because the presented Ni and Mn data have been measured from olivine crystals and the other aforementioned pyroxenite source indicators of pyroxenite sources rely on whole-rock geochemistry, it is important to be certain that the olivine phenocrysts are not xenocrysts from geochemically distinct parental magmas (i.e. introduced to meimechitic magmas by mixing). This aspect has been discussed in more detail elsewhere (Heinonen and Luttinen, 2010), but is summarized here for clarity: regardless of Fo content, the olivines contain 1) spinel inclusions with uniform geochemistry, 2) kaersutite-bearing crystallized melt inclusions, and 3) Ca and Ni contents that plot on a reasonable liquid line of descent. Given this evidence, it is very likely that all the primitive olivine phenocrysts crystallized from geochemically similar Mg-rich parental magmas derived from relatively uniform sources. In addition, we concentrate on samples that are not cumulates to discount the geochemical effects of accumulation on major and trace element compositions (see Heinonen and Luttinen, 2010).

Picrites from Gran Canaria show very similar X_{px} (Fig. 3) to the Karoo meimechites. In the following discussion, we will evaluate the consistency of this similarity (and its implication of similarly pyroxene-rich mantle sources) using the other petrological source indicators listed above. We emphasize, however, that the purpose of this study is not to study the origin of the Gran Canaria samples in detail – for such discussion, the reader is referred to, e.g., Gurenko et al. (2006, 2010) and references therein.

5.1.1. Zn/Fe

Le Roux et al. (2010) argued that elevated Zn/Fe of several OIBs is difficult to explain by melting of peridotitic mantle at varying temperature or pressure, but rather indicates sources rich in clinopyroxene and garnet (both fractionate Zn/Fe, unlike olivine and orthopyroxene). The Karoo meimechites exhibit Zn/Fe that is indistinguishable from MORB and peridotites and very similar to a hypothetical peridotite melt (Fig. 4). In contrast, Gran Canaria samples seem to be more closely associated with pyroxenite sources in terms of Zn/Fe (Fig. 4).

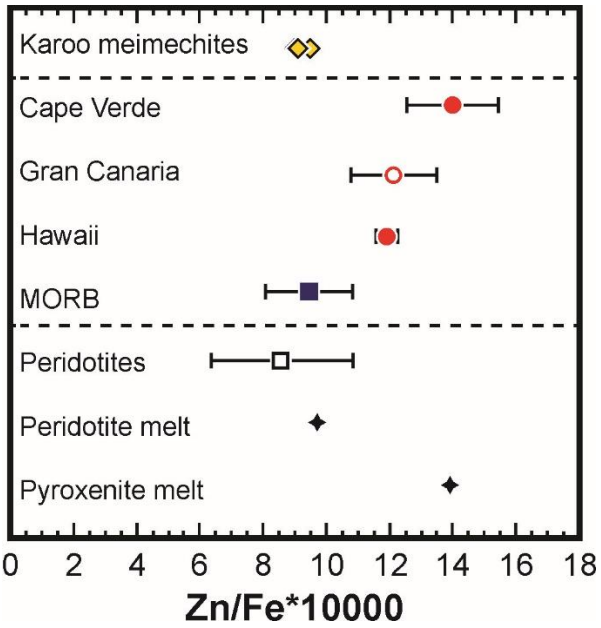

Figure 4. Karoo meimechites that are not cumulates (AL/B1b-03, AL/B7-03, and AL/B9-03; Heinonen and Luttinen, 2008; see also Heinonen and Luttinen, 2010) together with data from various geological settings and hypothetical melt compositions shown in whole-rock Zn/Fe*10^4 diagram. All data, except for the Karoo meimechites and Gran Canaria, are from Le Roux et al. (2010) with MORB and OIB suites fractionation-corrected to MgO = 12 wt.% (symbols represent averages and error bars are 1σ). Gran Canaria data only includes samples with MgO of 12 wt. % and has been compiled from GEOROC (http://georoc.mpchmainz.gwdg.de/georoc/). The Karoo meimechites represent olivine-controlled near-melt compositions (Heinonen and Luttinen, 2010) and, because olivine does not fractionate Zn/Fe (Le Roux et al., 2010), their compositions have not been corrected for fractionation.

5.1.2. MgO/CaO

On the basis of the melting behavior of fertile peridotite, Herzberg (2006) and Herzberg and Asimow (2008) suggested that the relationship of MgO and CaO could be used as a potential pyroxenite source indicator. Magmas from pyroxenite sources should generally exhibit lower CaO at a given MgO compared to magmas from peridotite sources (cf. Yang and Zhou, 2013). The Karoo meimechites plot in the peridotite melt field, although the most magnesian sample is very close to the hypothetical divide (Fig 5a). In comparison, the Gran Canaria samples analyzed by Sobolev et al. (2007) plot on both sides of the divide (Fig. 5a): the two Gran Canaria samples that exhibit the highest X_{px} (> 50%) plot below the divide in the pyroxenite melt field.

Importantly, experimental pyroxenite melts rarely exceed MgO contents of about 16 wt.% (see Yang and Zhou, 2013) and high olivine content or degree of melting are needed for this to happen (see, e.g., Kogiso et al., 2004). Based on the forsteritic olivines (up to Fo_{92}) found in the meimechites and parental melt calculations with PRIMELT software (Herzberg and Asimow, 2008), the parental melts of the Karoo meimechites had MgO contents in excess of 20 wt. %, probably around 25 wt. % (Fig. 5a; Heinonen and Luttinen, 2010). The parental melt compositions modeled with PRIMELT software are in equilibrium with a garnet-bearing peridotitic source rock (see Heinonen and Luttinen, 2010).

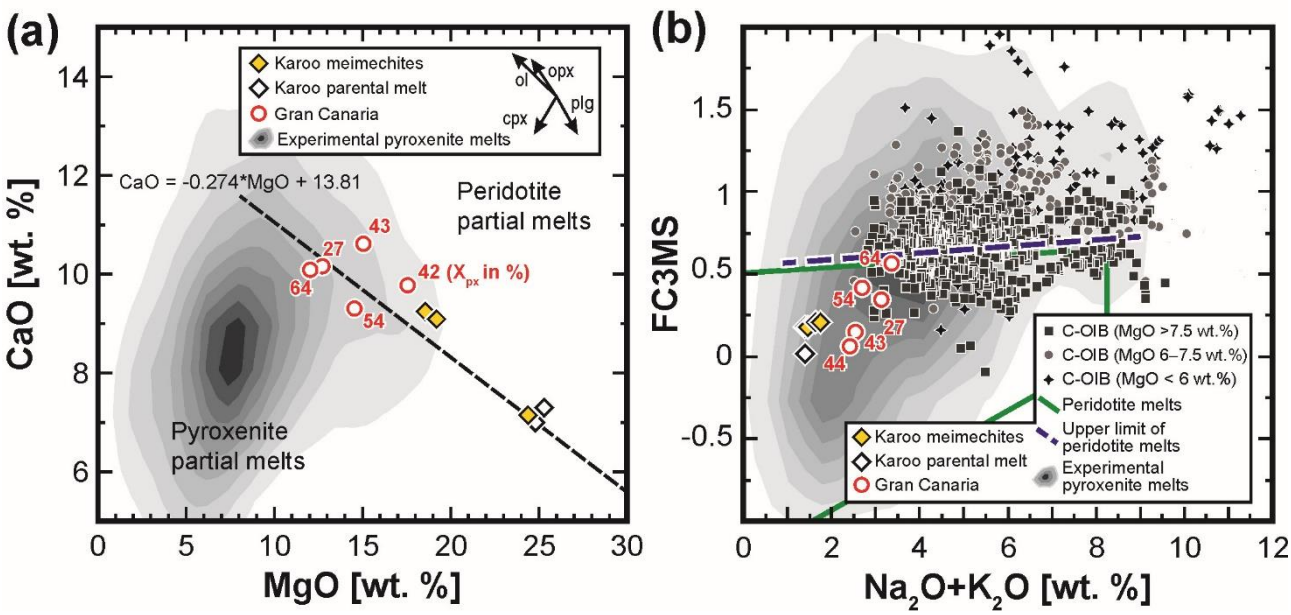

Figure 5. Karoo meimechites that are not cumulates (see Fig. 4) and their parental melt compositions (Heinonen and Luttinen, 2010), and Gran Canaria picrites that hosted or are closely related to the olivines analyzed by Sobolev et al. (2007) (samples G1265, GC59, GC35, 953C-93R-4_20-24, and 953C-101R-5_78-80; Schminke and Segschneider, 1998; Gurenko et al., 2006) shown in whole-rock (a) MgO [wt.%] vs. CaO [wt.%] and (b) $Na_2O + K_2O$ [wt.%] vs. FC3MS ($FeO^{tot}/CaO – 3*MgO/SiO_2$; all in wt.%) diagrams. Mn/Fe-based X_{px} values for the Gran Canaria samples, parental melt estimates for the Karoo meimechites (Heinonen and Luttinen, 2010), and experimental pyroxenite partial melt quantile contours at 10% intervals (based on a dataset compiled by Yang and Zhou, 2013) are included. In (a), fractionation vectors for olivine, orthopyroxene, clinopyroxene, and plagioclase, and the hypothetical line separating peridotite and pyroxenite partial melts (Herzberg and Asimow, 2008) are indicated. In (b), the data for continental OIB-like rocks (C-OIB), upper limit for peridotite melts, and peridotite partial melt fields are after Yang and Zhou (2013).

5.1.3. FC3MS

The FC3MS ($FeO^T/CaO – 3{*}MgO/SiO_2$; all in wt.%) source indicator was introduced by Yang and Zhou (2013) on the basis of parameterization of a considerable amount of previously published data on peridotite and pyroxenite melting experiments (Fig. 5b). The authors argue that effects of pressure and temperature on this parameter are insignificant (see also Yang et al., 2016). The Karoo

meimechites clearly plot in the field of peridotite melts in Fig. 5b. Gran Canaria samples also plot in the field of peridotite melts and close or within the field of continental OIB-like volcanic rocks (C-OIBs); again, the two samples having the highest X_{px} plot closer to the majority of pyroxenite partial melts.

5.1.4. Zr/Y vs. Nb/Y

Rather than being a direct indicator of pyroxenite sources, the Zr/Y vs. Nb/Y diagram can be considered an indicator of recycled eclogite sources (Fitton et al., 1997, 2003). It is largely based on the assumption that Nb is compatible in eclogite and is thus relatively and consistently depleted in normal MORBs derived from depleted upper mantle and enriched in OIBs derived from recycled sources. Plotting Nb/Y relative to Zr/Y helps in seeing through the effects of pressure and degree of melting on the partitioning of the different elements. The Nb systematics of the Karoo meimechites do not show evidence of recycled sources and they can be explained by low-degree high-pressure melting of sources similar to MORBs (Fig. 6). Gran Canaria samples plot in the OIB field and in or very close to the "Icelandic plume array" constrained by Fitton et al. (1997, 2003).

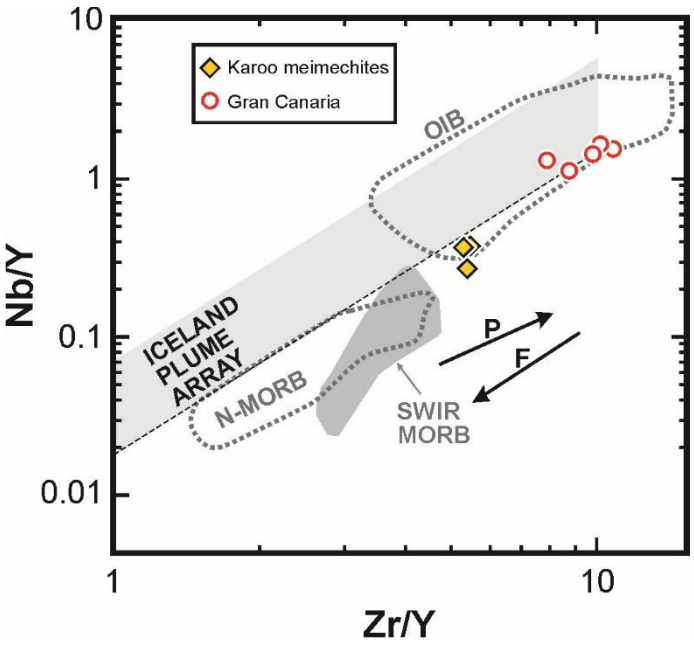

Figure 6. Karoo meimechites that are not cumulates and selected Gran Canaria picrites (see Figs. 4 and 5) shown in whole-rock Zr/Y vs. Nb/Y diagram. The Iceland Plume Array for Nb-enriched compositions and fields for N-MORB and OIB are after Fitton et al. (2003) and Fitton (2007). Data for SWIR MORBs compiled from PetDB (www.earthchem.org/petdb). P and F arrows denote the approximate effects of increasing pressure and degree of melting, respectively (Fitton et al., 1997).

5.1.5. Radiogenic isotopes

The Sr, Nd, Pb, and Os isotopic compositions of the Karoo meimechites are practically indistinguishable from those of Southwest Indian Ridge (SWIR) MORBs (or abyssal SWIR peridotites is terms of Os) and very similar to those of depleted MORB mantle (DMM) calculated at 180 Ma. This indicates their derivation from a dominantly peridotitic depleted mantle source without significant additions of enriched recycled materials (Fig. 7; Heinonen et al., 2010). The amount of recycled crust suggested by olivine Mn/Fe (X_{crc} = 10–31 %) would be expected to considerably shift the isotopic compositions towards those of OIBs that derive from enriched mantle (EM) domains (e.g., Pitcairn and Samoa; Fig. 7). In comparison, Gran Canaria basalts and picrites show variable isotopic compositions extending to highly radiogenic Sr and Pb, reflecting their derivation from complex mixtures of DMM, EM, and high-U/Pb (HIMU) sources (Fig. 7; e.g., Gurenko et al., 2006, 2010). Although not necessarily an indication of recycled sources, it is important to note that the

magmatic He isotopic composition of the Karoo meimechites is indistinguishable from that of SWIR MORBs as well (Heinonen and Kurz, 2015).

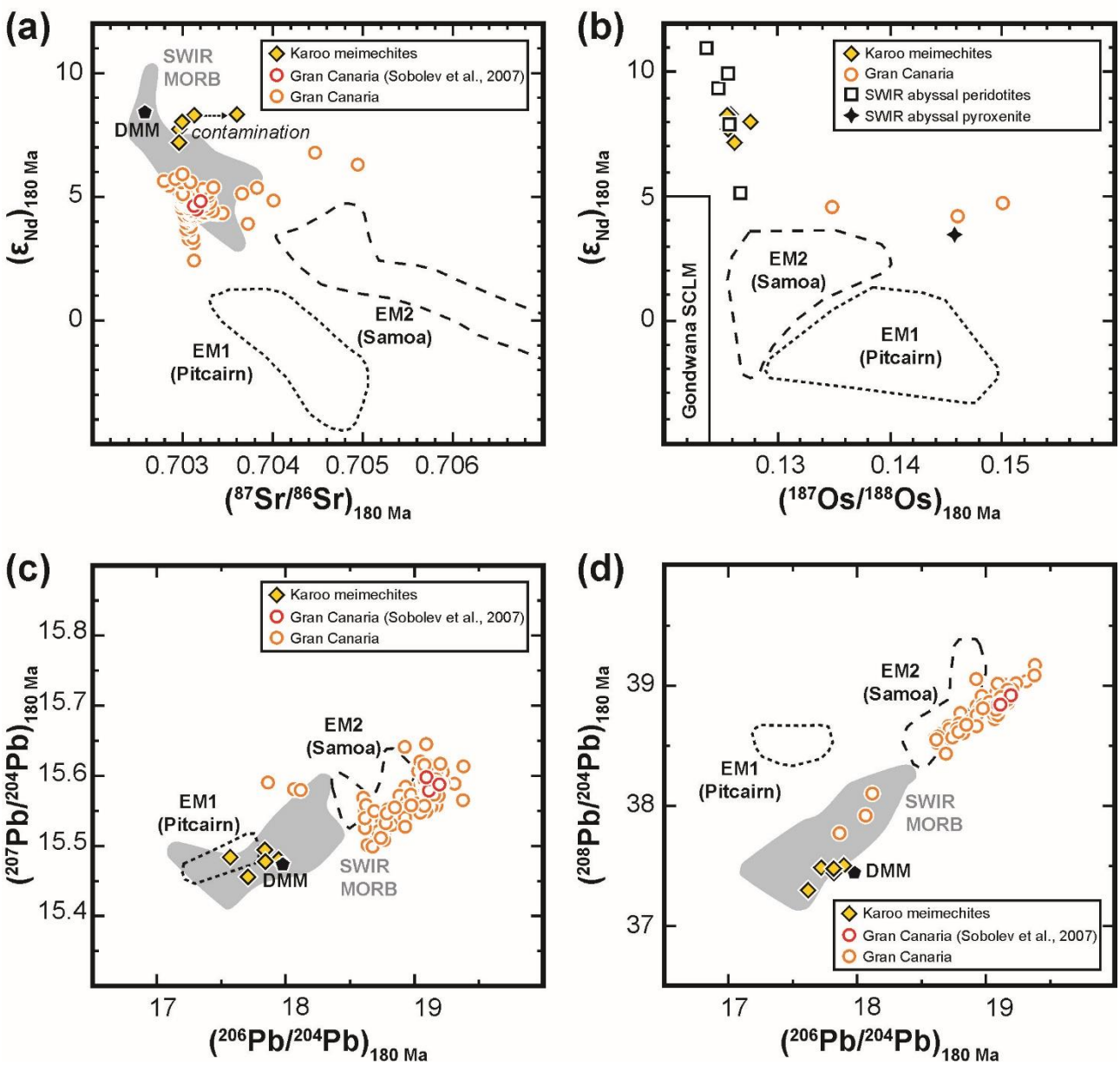

Figure 7. Karoo meimechites and related ferropicrites, and the estimated sources of the Gran Canaria basalts and picrites (samples G1265, GC59, and GC35 highlighted in a, c, and d; see Fig. 5), Pitcairn EM1 basalts, and Samoa EM2 basalts shown in (a) $^{87}Sr/^{86}Sr$ vs. ε_{Nd}, (b) $^{187}Os/^{188}Os$ vs. ε_{Nd}, c) $^{206}Pb/^{204}Pb$ vs. $^{207}Pb/^{204}Pb$, and (d) $^{206}Pb/^{204}Pb$ vs. $^{208}Pb/^{204}Pb$ diagrams at 180 Ma. Sr, Nd, Pb, and Os isotopic data for the OIBs compiled from GEOROC (http://georoc.mpchmainz.gwdg.de/georoc/; unpublished Nd isotopic data for Gran Canaria samples having Os isotopic data contributed by Kaj Hoernle). Depleted MORB mantle of Workman and Hart (2005) and representative SWIR MORB (compiled from PetDB, www.earthchem.org/petdb) sources shown for comparison in (a), (c), and (d). Estimates for Gondwana SCLM (the field extends outside of the diagram; Walker et al., 1989; Simon et al., 2007) and SWIR abyssal peridotites and pyroxenite (Warren et al., 2009; Day et al., 2017) shown for comparison in (b). All OIB, MORB, SCLM, and DMM data has been back-calculated at 180 Ma following the methods of Heinonen et al. (2010) for Os isotopes and Heinonen and Kurz (2015) for Sr, Nd, and Pb isotopes. In the case of SWIR abyssal peridotites and pyroxenite, Nd isotopic composition was back-calculated using Nd compositions corrected for ^{143}Nd ingrowth (Warren et al., 2009) and then using the method of Heinonen and Kurz (2015). Their Os isotopic compositions were back-calculated using $^{187}Re/^{188}Os$ reported by Day et al. (2017).

5.2. The plausibility of Ni and Mn/Fe in olivine as tracers of source mineralogy

Despite high Ni concentrations and low Mn/Fe in olivine, resulting in average X_{px} (52 %) and X_{crc} (16.8 %) values calculated on the basis of the latter, the Karoo meimechites exhibit considerable geochemical evidence of derivation from dominantly peridotitic depleted mantle sources similar to those of MORBs (namely SWIR MORBs; Figs. 4–7; see also Heinonen et al., 2010; Heinonen and Kurz, 2015). For comparison, Sobolev et al. (2007) suggest X_{px} and X_{crc} values of 10–15 % and 5 % for MORBs, respectively, although the data for MORB-related olivines reported by them spans a somewhat larger range in X_{px} values (Fig. 3).

It is evident that other processes than origin from pyroxenite are largely responsible for the relatively high Ni and low Mn/Fe in the Karoo meimechite olivines. Despite having similar isotopically depleted mantle sources, MORBs and Karoo meimechites exhibit evidence of distinct melting conditions and water contents in these sources. The relatively high Ni of Karoo meimechite olivines (Fig. 2) could be attributed to derivation at very high mantle pressures (~5–6 GPa) and temperatures (~1500–1600 °C) beneath the thick Gondwanan lithosphere, because such conditions favor low $K_D(Ni)^{ol\text{-}liq}$ in the source (see Matzen et al., 2013). These conditions have been determined with the help of Al-in-olivine thermometry, comparisons of the calculated parental melt compositions with peridotite partial melt compositions, and PRIMELT software (Heinonen and Luttinen, 2010; Heinonen et al., 2015). The difference in the temperature of formation relative to MORBs ($\Delta T \approx 200$ °C) is not far from that suggested for the Hawaiian tholeiites and MORBs ($\Delta T \approx 270$ °C; Putirka et al., 2007). High pressure also increases $K_D(Mn)^{ol\text{-}liq}$ (Matzen et al., 2017) and increase in source water contents increases $K_D(Mn)^{garnet\text{-}liq}$ (Balta et al., 2011). The presence of igneous kaersutite in olivine-hosted crystallized melt inclusions in the Karoo meimechites are evidence of relatively high water contents in their parental magmas (~1–2 wt. %; determined on the basis of the amount of kaersutite in the inclusions) and mantle sources (Heinonen and Luttinen, 2010). Furthermore, their high Sm/Yb ratios are evidence of garnet-bearing sources (Heinonen and Luttinen, 2008). Whereas MORBs derive dominantly from dry spinel-peridotite at low pressures (< 1 GPa; e.g., Langmuir et al., 1992), the Karoo meimechite parental melts were generated from water-enriched garnet-peridotite at high pressures, which could explain the relatively higher Ni contents and lower Mn/Fe in the latter.

The effects of the melting conditions and source water content on $K_D(Ni)^{ol\text{-}liq}$, $K_D(Mn)^{ol\text{-}liq}$, and $K_D(Mn)^{garnet\text{-}liq}$ are difficult to constrain quantitatively. Recently, Matzen et al. (2017) introduced a way to illustrate the effects of pressure (and temperature) of melting on Ni and Mn contents of olivine phenocrysts based on forward-modeling of peridotite partial melting. In a plot of MnO_{89} vs. NiO_{89} (MnO and NiO in olivine calculated at Fo_{89} based on liquid line of descent, see Matzen et al., 2017), the results of such models are able to replicate almost the full range of Mn and Ni variation of natural olivine phenocrysts from various tectonic settings (Fig. 8). In this diagram, the average olivines of the Karoo meimechites plot close to the high-pressure experiments, although they show a bit lower NiO_{89} than the experiments and most of the natural olivines at a given MnO_{89} (Fig. 8). This small difference could be attributed to possible additional influence of source water to $K_D(Mn)^{garnet\text{-}liq}$, but we do not speculate about it further, as this effect has not been constrained in detail (see Balta et al., 2011). Nevertheless, based on this diagram, the high pressure of peridotite melting alone may already be able to explain the elevated Ni and Mn in the olivine phenocrysts of the Karoo meimechites.

Our study highlights the importance of relying on multiple pyroxenite tracers in unraveling the sources of Mg-rich volcanic rocks (see Yang et al., 2016) and implies that X_{px} values calculated with the method of Sobolev et al. (2007) are very likely to be false for many volcanic rocks erupted on thick lithosphere. If using Ni and Mn/Fe of olivine phenocrysts for the purpose of recognizing source rocks, the conditions of formation for the suites under inspection should be relatively similar. In such cases, they may be useful in qualitative comparisons and correlations with other pyroxenite source indicators and radiogenic isotopes should be expected (see, e.g., Sobolev et al., 2008; Gurenko et al., 2009, 2013; Heinonen et al., 2013).

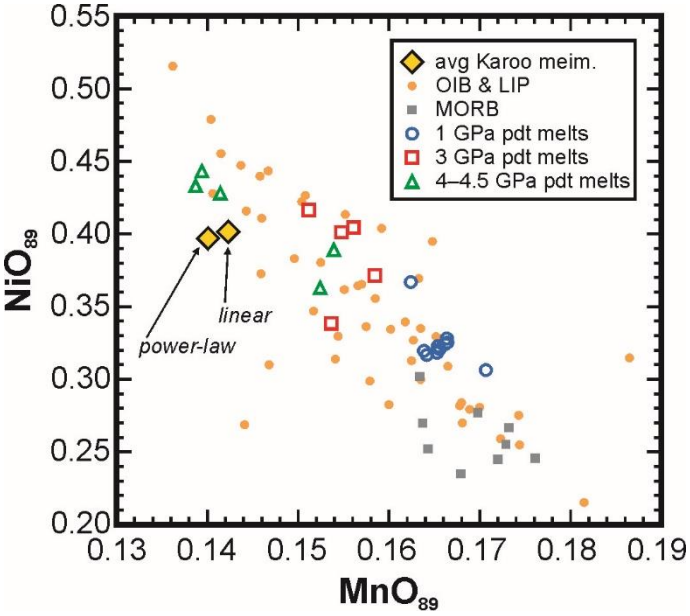

Figure 8. Comparison of model peridotite melting results (1–4.5 GPa) to natural olivine phenocryst compositions (Karoo meimechites, OIB & LIP, and MORB) in olivine MnO vs. NiO plot corrected to Fo content of 89 mol. %. For calculation of MnO_{89} and NiO_{89} and original data (excluding those of Karoo meimechites presented in this study) see Matzen et al. (2017). For the Karoo meimechites, averages of the two samples calculated at Fo_{89} with linear and power-law functions (see Matzen et al., 2017) are shown.

Acknowledgements

We warmly thank the reviewers (Véronique Le Roux, Andrew K. Matzen, and an anonymous one) and Editor (Klaus Mezger) for providing clear and thoughtful commentary with the help of which the manuscript was improved. We are also grateful to Thomas Wagner for making this study possible by acquiring state-of-the-art LA-ICP-MS for our department and Radoslaw Michallik for helping with the EPMA analysis. We give special thanks to Helena Korkka for assisting with the separation and mount procedures – we thank you for good work and company over the years and wish you a retirement filled with happiness. Thanks to Zong-Feng Yang and Kaj Hoernle for providing geochemical data for comparison. The administrators and updaters of the geochemical data service GEOROC (http://georoc.mpch-mainz.gwdg.de/georoc/) are thanked for their important and hard work. This study has been supported by the Department of Geosciences and Geography, University of Helsinki.

Supplementary Electronic Materials

1. Evaluation of data quality and accuracy of LA-ICP-MS method (text and figures)
2. Full LA-ICP-MS dataset (table)
3. Full EPMA dataset (table)

References

Arndt, N.T., Lehnert, K., Vasil'ev, Y., 1995. Meimechites: highly magnesian lithosphere-contaminated alkaline magmas from deep subcontinental mantle. Lithos 34, 41–59. https://doi.org/10.1016/0024-4937(95)90009-8

Balta, J.B., Asimow, P.D., Mosenfelder, J.L., 2011. Manganese partitioning during hydrous melting of peridotite. Geochim. Cosmochim. Acta 75, 5819–5833. https://doi.org/10.1016/j.gca.2011.05.026.

Day, J.M.D., Walker, R.J., Warren, J.M., 2017. ^{186}Os–^{187}Os and highly siderophile element abundance systematics of the mantle revealed by abyssal peridotites and Os-rich alloys. Geochim. Cosmochim. Acta 200, 232–254. https://doi.org/10.1016/j.gca.2016.12.013.

Ellam, R.M., 2006. New constraints on the petrogenesis of the Nuanetsi picrite basalts from Pb and Hf isotope data. Earth Planet. Sci. Lett. 245, 153–161. https://doi.org/10.1016/j.epsl.2006.03.004

Fitton, J.G., 2007. The OIB paradox. Geological Society of America Special Papers 430, 387–412. https://doi.org/10.1130/2007.2430(20).

Fitton, J.G., Saunders, A.D., Norry, M.J., Hardarson, B.S., Taylor, R.N., 1997. Thermal and chemical structure of the Iceland Plume. Earth Planet. Sci. Lett. 153, 197–208. https://doi.org/10.1016/s0012-821x(97)00170-2.

Fitton, J.G., Saunders, A.D., Kempton, P.D., Hardarson, B.S., 2003. Does depleted mantle form an intrinsic part of the Iceland Plume? Geochem. Geophys. Geosyst. 4, https://doi.org/10.1029/2002gc000424.

Garcia, M.O., Weis, D., Swinnard, L., Ito, G., Pietruszka, A.J., 2015. Petrology and Geochemistry of Volcanic Rocks from the South Kaua`i Swell Volcano, Hawai`i: Implications for the Lithology and Composition of the Hawaiian Mantle Plume. J. Petrol. 56, 1173–1197. https://doi.org/10.1093/petrology/egv033

Guillong, M., Meier, D.L., Allan, M.M., Heinrich, C.A., Yardley, B.W.D., 2008. SILLS: A MATLAB-based program for the reduction of laser ablation ICP-MS data of homogeneous materials and inclusions. In: Sylvester, P. (Ed.), Laser Ablation ICP–MS in the Earth Sciences: Current Practices and Outstanding Issues. Mineralogical Association of Canada, Québec, pp. 328–333.

Gurenko, A.A., Hoernle, K.A., Hauff, F., Schmincke, H.-U., Han, D., Miura, Y.N., Kaneoka, I., 2006. Major, trace element and Nd–Sr–Pb–O–He–Ar isotope signatures of shield stage lavas from the central and western Canary Islands: Insights into mantle and crustal processes. Chem. Geol. 233, 75–112. https://doi.org/10.1016/j.chemgeo.2006.02.016.

Gurenko, A.A., Sobolev, A.V., Hoernle, K.A., Hauff, F., Schmincke, H., 2009. Enriched, HIMU-type peridotite and depleted recycled pyroxenite in the Canary plume: A mixed-up mantle. Earth Planet. Sci. Lett. 277, 514–524. https://doi.org/10.1016/j.epsl.2008.11.013.

Gurenko, A.A., Hoernle, K.A., Sobolev, A.V., Hauff, F., Schmincke, H., 2010. Source components of the Gran Canaria (Canary Islands) shield stage magmas: evidence from olivine composition and Sr-Nd-Pb isotopes. Contrib. Mineral. Petrol. 159, 689–702. https://doi.org/10.1007/s00410-009-0448-8.

Gurenko, A.A., Geldmacher, J., Hoernle, K.A., Sobolev, A.V., 2013. A composite, isotopically-depleted peridotite and enriched pyroxenite source for Madeira magmas: Insights from olivine. Lithos 170–171, 224–238. https://doi.org/10.1016/j.lithos.2013.03.002.

Heinonen, J.S., Kurz, M.D., 2015. Low-$^{3}He/^{4}He$ sublithospheric mantle source for the most magnesian magmas of the Karoo large igneous province. Earth Planet. Sci. Lett. 426, 305–315. https://doi.org/10.1016/j.epsl.2015.06.030.

Heinonen, J.S., Luttinen, A.V., 2008. Jurassic dikes of Vestfjella, western Dronning Maud Land, Antarctica: Geochemical tracing of ferropicrite sources. Lithos 105, 347–364. https://doi.org/10.1016/j.lithos.2008.05.010.

Heinonen, J.S., Luttinen, A.V., 2010. Mineral chemical evidence for extremely magnesian subalkaline melts from the Antarctic extension of the Karoo large igneous province. Miner. Petrol. 99, 201–217. https://doi.org/10.1007/s00710-010-0115-9.

Heinonen, J.S., Carlson, R.W., Luttinen, A.V., 2010. Isotopic (Sr, Nd, Pb, and Os) composition of highly magnesian dikes of Vestfjella, western Dronning Maud Land, Antarctica: A key to the origins of the Jurassic Karoo large igneous province? Chem. Geol. 277, 227–244. https://doi.org/10.1016/j.chemgeo.2010.08.004.

Heinonen, J.S., Luttinen, A.V., Riley, T.R., Michallik, R.M., 2013. Mixed pyroxenite–peridotite sources for mafic and ultramafic dikes from the Antarctic segment of the Karoo continental flood basalt province. Lithos 177, 366–380. https://doi.org/10.1016/j.lithos.2013.05.015.

Heinonen, J.S., Jennings, E.S., Riley, T.R., 2015. Crystallisation temperatures of the most Mg-rich magmas of the Karoo LIP on the basis of Al-in-olivine thermometry. Chem. Geol. 411, 26–35. http://dx.doi.org/10.1016/j.chemgeo.2015.06.015.

Heinonen, J,S., Luttinen A,V., Bohrson W.A., 2016. Enriched continental flood basalts from depleted mantle melts: modeling the lithospheric contamination of Karoo lavas from Antarctica. Contrib. Mineral. Petrol. 171:9. https://doi.org/10.1007/s00410-015-1214-8

Heinrich, C.A., Pettke, T., Halter, W.E., Aigner-Torres, M., Audétat, A., Günther, D., Hattendorf, B., Bleiner, D., Guillong, M., Horn, I., 2003. Quantitative multi-element analysis of minerals, fluid and melt inclusions by laser-ablation inductively-coupled-plasma mass-spectrometry. Geochim. Cosmochim. Acta 67, 3473–3497. https://doi.org/10.1016/S0016-7037(03)00084-X.

Herzberg, C., 2006. Petrology and thermal structure of the Hawaiian plume from Mauna Kea volcano. Nature 444, 605–609. https://doi.org/10.1038/nature05254.

Herzberg, C., Asimow, P.D., 2008. Petrology of some oceanic island basalts: PRIMELT2.XLS software for primary magma calculation. Geochem. Geophys. Geosyst. 9. https://doi.org/10.1029/2008GC002057.

Hofmann, A.W., White, W.M., 1982. Mantle plumes from ancient oceanic crust. Earth and Planet. Sci. Lett. 57, 421–436. https://doi.org/10.1016/0012-821x(82)90161-3

Jacobs, J., Pisarevsky, S., Thomas, R.J., Becker, T., 2008. The Kalahari Craton during the assembly and dispersal of Rodinia. Precambrian Res. 160, 142–158. https://doi.org/10.1016/j.precamres.2007.04.022.

Jochum, K.P., Nohl, U., Herwig, K., Lammel, E., Stoll, B., Hofmann, A.W., 2005. GeoReM: A New Geochemical Database for Reference Materials and Isotopic Standards. Geostandards and Geoanalytical Research 29, 333–338. https://doi.org/10.1111/j.1751-908X.2005.tb00904.x.

Jourdan, F., Féraud, G., Bertrand, H., Kampunzu, A.B., Tshoso, G., Watkeys, M.K., Le Gall, B., 2005. Karoo large igneous province: Brevity, origin, and relation to mass extinction questioned by new $^{40}Ar/^{39}Ar$ age data. Geology 33, 745–748. https://doi.org/10.1130/g21632.1

Jourdan, F., Féraud, G., Bertrand, H., Watkeys, M.K., 2007. From flood basalts to the inception of oceanization: example from the $^{40}Ar/^{39}Ar$ high-resolution picture of the Karoo large igneous province. Geochem. Geophys. Geosyst. 8, https://doi.org/10.1029/2006GC001392.

Kamenetsky, V.S., Chung, S., Kamenetsky, M.B., Kuzmin, D.V., 2012. Picrites from the Emeishan Large Igneous Province, SW China: a Compositional Continuum in Primitive Magmas and their Respective Mantle Sources. J. Petrol. 53, 2095–2113. https://doi.org/10.1093/petrology/egs045.

Kogiso, T., Hirschmann, M.M., Reiners, P.W., 2004. Length scales of mantle heterogeneities and their relationship to ocean island basalt geochemistry. Geochim. Cosmochim. Acta 68, 345–360. https://doi.org/10.1016/S0016-7037(03)00419-8.

Langmuir, C.H., Klein, E.M., Plank, T., 1992. Petrological systematics of mid-ocean ridge basalts: constraints on melt generation beneath ocean ridges. In: Morgan, J.P., Blackman, D.K., Sinton, J.M. (Eds.), Mantle Flow and Melt Generation at Mid-Ocean Ridges. In: Geophys. Monogr., vol.71. AGU, pp.183–280.

Le Bas, M.J., 2000. IUGS reclassification of the high-Mg and picritic volcanic rocks. J. Petrol. 41, 1467–1470. https://doi.org/10.1093/petrology/41.10.1467

Le Roux, V., Lee, C.A., Turner, S.J., 2010. Zn/Fe systematics in mafic and ultramafic systems: implications for detecting major element heterogeneities in the Earth's mantle. Geochim. Cosmochim. Acta 74, 2779–2796. https://doi.org/10.1016/j.gca.2010.02.004.

Li, C., Ripley, E.M., 2010. The relative effects of composition and temperature on olivine-liquid Ni partitioning: Statistical deconvolution and implications for petrologic modeling. Chem. Geol. 275, 99–104. https://doi.org/10.1016/j.chemgeo.2010.05.001.

Luttinen, A.V., Heinonen, J.S., Kurhila, M., Jourdan, F., Mänttäri, I., Vuori, S., Huhma, H., 2015. Depleted mantle-sourced CFB magmatism in the Jurassic Africa–Antarctica rift: petrology and $^{40}Ar/^{39}Ar$ and U/Pb chronology of the Vestfjella dyke swarm, Dronning Maud Land, Antarctica. J. Petrol. 56, 919–952. http://dx.doi.org/10.1093/petrology/egv022.

Luttinen, A.V., Siivola, J.U., 1997. Geochemical characteristics of Mesozoic lavas and dikes from Vestfjella, Dronning Maud Land: recognition of three distinct chemical types. In: Ricci, C.A. (Ed.), The Antarctic Region: Geological Evolution and Processes. Siena: Terra Antarctica Publications, Italy, pp. 495–503.

Matzen, A.K., Baker, M.B., Beckett, J.R., Stolper, E.M., 2013. The Temperature and Pressure Dependence of Nickel Partitioning between Olivine and Silicate Melt. J. Petrol. 54, 2521–2545. https://doi.org/10.1093/petrology/egt055.

Matzen, A.K., Wood, B.J., Baker, M.B., Stolper, E.M., 2017. The roles of pyroxenite and peridotite in the mantle sources of oceanic basalts. Nat. Geosci. 10, 530–535. https://doi.org/10.1038/NGEO2968

Niu, Y., Wilson, M., Humphreys, E.R., O'Hara, M.J., 2011. The Origin of Intra-plate Ocean Island Basalts (OIB): the Lid Effect and its Geodynamic Implications. J. Petrol. 52, 1443–1468. https://doi.org/10.1093/petrology/egr030.

Pettke, T., Oberli, F., Audétat, A., Guillong, M., Simon, A.C., Hanley, J.J., Klemm, L.M., 2012. Recent developments in element concentration and isotope ratio analysis of individual fluid inclusions by laser ablation single and multiple collector ICP-MS. Ore Geol. Rev. 44, 10–38. https://doi.org/10.1016/j.oregeorev.2011.11.001.

Pouchou, J.L. & Pichoir, F. 1985. "PAP" procedure for improved quantitative microanalysis. In: Armstrong, J.T. (Ed.), Microbeam Analysis. San Francisco Press, San Francisco, United States, pp. 104–106.
Putirka, K.D., 1999. Melting depths and mantle heterogeneity beneath Hawaii and the East Pacific Rise: constraints from Na/Ti and rare earth element ratios. J. Geophys. Res. 104 (B2), 2817–2829. https://doi.org/10.1029/1998jb900048

Putirka, K.D., Perfit, M., Ryerson, F.J., Jackson, M.G., 2007. Ambient and excess mantle temperatures, olivine thermometry, and active vs. passive upwelling. Chem. Geol. 241, 177–206. https://doi.org/10.1016/j.chemgeo.2007.01.014.

Putirka, K., Ryerson, F.J., Perfit, M., Ridley, W.I., 2011. Mineralogy and Composition of the Oceanic Mantle. J. Petrol. 52, 279–313. https://doi.org/10.1093/petrology/egq080.

Schminke, H.-U., Segschneider, B., 1998. Shallow submarine to emergent basaltic shield volcanism of Gran Canaria: Evidence from drilling into the volcanic apron. In: Weaver, P.P.E., Schminke, H.-U., Firth, J.V., Duffield, W. (Eds.), Proceedings of the Ocean Drilling Program, Scientific Results. Ocean Drilling Program, College Station, TX, United States, pp. 141–181. https://doi.org/10.2973/odp.proc.sr.157.110.1998

Simon, N.S., Carlson, R.W., Graham Pearson, D., Davies, G.R., 2007. The origin and evolution of the Kaapvaal cratonic lithospheric mantle. J. Petrol. 48, 589–625. https://doi.org/10.1093/petrology/egl074.

Søager, N., Portnyagin, M., Hoernle, K., Holm, P.M., Hauff, F., Garbe-Schönberg, D., 2015. Olivine Major and Trace Element Compositions in Southern Payenia Basalts, Argentina: Evidence for Pyroxenite - Peridotite Melt Mixing in a Back-arc Setting. J. Petrol. 56, 1495–1518. https://doi.org/10.1093/petrology/egv043

Sobolev, A.V., Hofmann, A.W., Sobolev, S.V., Nikogosian, I.K., 2005. An olivine-free mantle source of Hawaiian shield basalts. Nature 434, 590–597. https://doi.org/10.1038/nature03411.

Sobolev, A.V., Hofmann, A.W., Kuzmin, D.V., Yaxley, G.M., Arndt, N.T., Chung, S., Danyushevsky, L.V., Elliott, T., Frey, F.A., Garcia, M.O., Gurenko, A.A., Kamenetsky, V.S., Kerr, A.C., Krivolutskaya, N.A., Matvienkov, V.V., Nikogosian, I.K., Rocholl, A., Sigurdsson, I.A., Sushchevskaya, N.M., Teklay, M., 2007. The amount of recycled crust in sources of mantle-derived melts. Science 316, 412–417. https://doi.org/10.1126/science.1138113.

Sobolev, A.V., Hofmann, A.W., Brügmann, G., Batanova, V.G., Kuzmin, D.V., 2008. A quantitative link between recycling and osmium isotopes. Science 321, 536. https://doi.org/10.1126/science.1158452.

Spandler, C., Pettke, T., Rubatto, D., 2011. Internal and External Fluid Sources for Eclogite-facies Veins in the Monviso Meta-ophiolite, Western Alps: Implications for Fluid Flow in Subduction Zones. J. Petrol. 52, 1207–1236. https://doi.org/10.1093/petrology/egr025

Walker, R.J., Carlson, R.W., Shirey, S.B., Boyd, F.R., 1989. Os, Sr, Nd, and Pb isotope systematics of Southern African peridotite xenoliths: Implications for the chemical evolution of subcontinental mantle. Geochim. Cosmochim. Acta 53, 1583–1595. https://doi.org/10.1016/0016-7037(89)90240-8.

Warren, J.M., Shimizu, N., Sakaguchi, C., Dick, H.J.B., Nakamura, E., 2009. An assessment of upper mantle heterogeneity based on abyssal peridotite isotopic compositions. J. Geophys. Res. 114 (B12), https://doi.org/10.1029/2008JB006186.

Workman, R.K., Hart, S.R., 2005. Major and trace element composition of the depleted MORB mantle (DMM). Earth Planet. Sci. Lett. 231, 53–72. https://doi.org/10.1016/j.epsl.2004.12.005.

Yang, Z., Zhou, J., 2013. Can we identify source lithology of basalt? Scientific Reports 3, 1856. https://doi.org/10.1038/srep01856

Yang, Z., Li, J., Liang, W., Luo, Z., 2016. On the chemical markers of pyroxenite contributions in continental basalts in Eastern China: Implications for source lithology and the origin of basalts. Earth-Sci. Rev. 157, 18–31.